



Optical sensing and analyte manipulation in solid-state nanopores

Journal:	<i>Analyst</i>
Manuscript ID:	AN-MRV-12-2014-002388.R1
Article Type:	Minireview
Date Submitted by the Author:	02-Feb-2015
Complete List of Authors:	Gilboa, Tal; Technion-IIT, Biomedical Engineering Meller, Amit; Technion -IIT, Biomedical Engineering; Boston University, Biomedical Engineering

Optical sensing and analyte manipulation in solid-state nanopores

Tal Gilboa and Amit Meller

Department of Biomedical Engineering

The Technion – Israel Institute of Technology

Haifa, Israel 32000

Abstract:

The field of nanopore sensing have gained increasing attention. Much progress has been made towards biotechnological applications that involve electrical measurements of temporal changes in the ionic current flowing through the pore. But in many cases the electrical signal is restricted by the non-ideal noise components, limited throughput, and insufficient temporal or spatial resolutions. To address these limitations, high-sensitivity optical detection techniques that complement the electrical measurements have been developed. The optical techniques involve high-bandwidth, multicolor and high-throughput measurements. Here we review recent advancements and developments taking place in the field of optical sensing in solid-state nanopores. We describe the main optical methods used in this field involving total internal reflection and confocal microscopy in addition to sophisticated background suppression strategies. We further present the phenomenon of light induced analytes manipulation at the pore and the contribution of the optical sensing approach to possible nanopore sensing applications such as, optical based DNA sequencing using nanopores.

i. Introduction

Nanopores are an emerging class of single-molecule biosensors, that has attracted increasing attention in the past decade due to three prominent features: (i) extremely high sensitivity, with the ability to detect as low as a few atto-moles of DNA molecules [1], (ii) versatility in terms of the different biomolecules it can probe, including DNA, RNA and proteins [2, 3], as well as its (iii) compact and miniature form factor, which lends itself to portable, point-of-care applications [4]. Solid-state nanopore sensors are composed of an ultrathin insulating membrane, typically only a few nanometers thick, in which a nanoscale pore or arrays containing multiple pores are formed [5]. The size of the nanopore can be tailored with subnanometer precision, to match the target analyte size [6-8]. Specifically, small nanopores in the size range of 2 nm to 20 nm, which are the focus of this review, have been broadly utilized to ensure single-file threading of individual biomolecules [4, 9]. The thin membrane separates two liquid chambers containing either symmetrical or asymmetrical salt solution. To date, most works employed electrical ion-current measurements to detect and characterize biomolecule entry into and passage through the nanopores. Electrical sensing in nanopores has been utilized for a variety of sensing applications in biotechnology [10], most prominently for direct, single-molecule nucleic acid sequencing [11-18], probing of RNA structures [15, 19-21], probing of proteins [3, 22, 23] and genotyping of viral genes [24, 25].

In recent years, substantial progress has been made to improve the performance of nanopore sensors, particularly in their capacity to distinguish between fine macromolecular properties [26]. For example, design of nanopore-based sequencing which can distinguish each of the four different nucleotides in a single-stranded DNA strand as it translocates through the pore, has been a major goal in a number of studies. However, to date the development of real-life applications employing electrical sensing of solid-state nanopores has been stunted by three major factors:

(i) Noise and bandwidth: In a typical nanopore set up, the temporal resolution is limited to 1-10 μ s due to the limited signal bandwidth of each element involved in the current measurements. Furthermore, the electrical signal is hindered by non-ideal ion current noise spectra, which involves low frequency (1/f) flicker noise as well as high frequency dielectric loss and capacitive noise, on top of the flat thermal noise (Johnson-Nyquist) and electronic shot noise [27-30]. These noise components are generally believed to be the key limiting factors of the technique's ability to resolve fine molecular features, as required in many sensing applications.

1
2
3 (ii) Throughput: The ability to process many biomolecules simultaneously is critical
4 for numerous bio-technological applications, such as DNA sequencing, RNA expression
5 analyses. Simultaneous multiplexed readout from hundreds if not thousands of nanopores,
6 without compromising the detection bandwidth and sensitivity, poses a central challenge
7 in nanopore sensing design [31].
8
9

10
11
12 (iii) Spatial information and spatial resolution: The typical nanopore channel is a few
13 nanometers long. However, many molecular (i.e., a DNA nucleotide) are only a fraction of
14 a nanometer in size, warranting development of strategies to further improve the
15 nanopore spatial resolution.
16
17

18
19 A number of strategies have been proposed to address these limitations. In many
20 cases, the improved approaches involve supplementation of the electrical ion
21 measurement with additional electrical measurements. For example, integration of a pair
22 of local nano-electrodes capable of injecting electrical current along the nanopore
23 perimeter which is modulated by the biomolecule as it translocates through the pore [32]
24 could provide a mean to detect fine molecular features of the translocating molecule.
25 Similarly employment of an atomically thin substrate, such as graphene could improve the
26 spatial resolution of the nanopore [33-36].
27
28
29
30
31
32

33 Another approach, which is at the focus of this review paper, involves
34 complementation of the electrical sensing with high sensitivity optical detection. This
35 approach is particularly powerful, in that it provides a measurement fundamentally
36 independent of the electrical sensing, that relies on photons rather than electrons.
37 Importantly, optical sensing can be performed at the far-field, as photons (unlike electrons
38 or ions) freely travel in the aqueous media surrounding the nanopores. This adjunctive
39 feature opens up vast opportunities for light excitations and broad spectral emission,
40 which will impose minimal interference with the local electrical measurement performed at
41 the nanopore itself. Moreover, incorporation of optical sensing in nanopores introduces
42 the benefits of a wealth of high-performance reagents, such as high-brightness
43 fluorophores covering a broad spectral range, high-sensitivity sensors, including
44 Avalanche Photo Diodes (APDs), Electron-Multiplying and Scientific CMOS CCD cameras
45 and ultra-compact solid-state light sources spanning the near UV to the IR wavelength
46 regimes and other components developed for single-molecule optical sensing.
47
48
49
50
51
52
53
54
55

56 This review will first describe the most prominent optical methods employed for
57 background noise suppression. Approaches designed to provide further background
58 suppression will then be detailed. The second section of this review is devoted to the use
59 of Ca^{2+} -activated dyes, which are used as independent ion probes either in addition to or
60

1
2
3 in place of direct ion current measurements. Probing fluorescence emitted by the Ca²⁺-
4 activated dyes yield signals highly localized to the pore vicinity and is less affected by
5 charge fluctuations in the system, as compared to 'classical' ion current probing. The third
6 section is dedicated to optical methods used to manipulate analytes at the nanopore.
7 Specifically, we discuss methods to control the DNA or proteins translocation velocity by
8 light. We then describe nanopore based optical DNA sequencing as an example for bio-
9 sensing application that utilizes optical sensing. We finally end with a discussion and
10 outlook for further improvements and developments in this field.
11
12
13
14
15
16
17
18

19 ii. Optical approaches for single-molecule detection in solid-state 20 nanopores 21

22 A principle common to essentially all optical-based single-molecule detection
23 methods is the basic requirement to suppress the level of the background light to levels
24 that permit detection of a *single fluorophore*. Here, we discuss two common methods that
25 have been extensively used in single-molecule sensing, particularly for the detection of
26 surface-immobilized biomolecules. Notably, adaptation of these methods for their
27 combined use with solid-state nanopores has presented some non-trivial experimental
28 challenges discussed here.
29
30
31
32
33

34 1. TIRF illumination 35

36 In total internal reflection fluorescence (TIRF), the excitation light is introduced from
37 a higher refractive index medium to a lower refractive index medium at an angle slightly
38 larger than the critical angle of incidence; thus the light is fully internally reflected at the
39 interface of the two media [37]. Consequently, an exponentially decaying electromagnetic
40 field (an evanescent field) is formed close to the interface, restricting the excitation of
41 molecules to this narrow region and resulting in significantly less background light.
42 Furthermore, since large surfaces can be excited using TIR, wide-field imaging devices
43 (i.e., EM-CCDs) can be used for parallel imaging of many molecules. Two main approaches
44 have been developed for TIRF microscopy. In the prism-based approach, a small glass
45 prism facilitates the introduction of the laser beam at an angle larger than the critical
46 angle formed at the glass-water interface. The emitted light is imaged from the opposite
47 side, by means of a long working distance objective. In the objective-based approach, a
48 particularly high NA microscope objective (typically NA >1.40) is illuminated with a
49 focused laser beam at its back focal plane at an off-axis point, creating a tilted collimated
50 beam at the sample side. The tilting angle can be adjusted by simply controlling the offset
51 distance of the laser beam at the objective back focal plane, to generate TIR illumination.
52
53
54
55
56
57
58
59
60

1
2
3 One of the challenges for adapting conventional TIRF approaches to the nanopore
4 system is posed by the fact that the ultra-thin solid membrane where the TIR should be
5 formed, must be immersed in liquid buffer on both of its sides. While the nanopore
6 membrane (typically silicon nitride) possesses a high index of refraction (about 2.0) [38], its
7 ultra-thin thickness (~ 10 nm) renders it nearly transparent, and TIR cannot be formed in
8 the common solid-liquid interface configuration. In 2010, Soni and coworkers proposed a
9 simple solution to this issue by introducing asymmetric fluids at the *cis* and *trans* chambers
10 [39]. Specifically, the index of refraction of the *trans* chamber solution (n_{trans}) was adjusted
11 such that: $n_{cis} < n_{trans} < n_{glass}$, enabling generation of TIR at the SiN_x membrane, preventing
12 light from progressing into the *cis* chamber where labeled biomolecules were introduced;
13 overall, the background light emitted by molecules residing in the vicinity of the
14 membrane, as well as scattered light from the buffer solution were reduced.
15
16
17
18
19
20
21
22

23 In addition, Soni and coworkers successfully synchronized the electrical signal with
24 the optical signals for the first time, thereby providing exact timing of each camera frame
25 in sync with the ion current A/D sampling. In order to find the nanopore position on the
26 SiN_x membrane, they took advantage of the fact that unlike the random behavior of
27 background fluorescent spots, the fluorescence signal from the pore is stationary and
28 lights up in synchrony with the electrical signal. Thus, the pixel corresponding to the pore
29 location will, over time, accumulate the highest fluorescence intensity. Simple summation
30 of all images captured during translocation of a fluorescently labeled molecule through
31 the nanopore, yields a clear peak, which corresponds to the pore position on the CCD.
32 This procedure was utilized to trace the fluorescence intensity at the nanopore position
33 over time. In this study, a ~ 400 bp DNA fragments each labeled randomly with 5 Alexa647
34 fluorophores were translocated through a 4 nm pore. The synchronous electrical and
35 optical events (Fig 1) clearly show that an optical signal can be obtained from the fast
36 moving DNA molecules. Statistical analysis of hundreds of translocations events showed an
37 optical signal to noise ratio > 2 .
38
39
40
41
42
43
44
45
46
47

48 2. Confocal illumination

49

50 In confocal imaging, the excitation laser beam is focused to a diffraction-limited spot
51 and the emitted light at that spot is focused onto a spatial pinhole to reject out of focus
52 light [40]. The light passing through the pinhole is then focused onto a point-like detector,
53 such as an APD. High numerical aperture water immersion objectives are often used to
54 minimize spherical aberrations. In the case of nanopore sensing, the pore must be
55 precisely positioned, in three dimensions, at the confocal spot to maximize the detection
56 efficiency.
57
58
59
60

1
2
3
4
5
6
7
8
9
10
11
12
13
14
15
16
17
18
19
20
21
22
23
24
25
26
27
28
29
30
31
32
33
34
35
36
37
38
39
40
41
42
43
44
45
46
47
48
49
50
51
52
53
54
55
56
57
58
59
60

Di Fiori and coworkers integrated confocal measurements with solid-state nanopore biosensing [41]. They focused an expanded 532 nm laser beam on the SiN_x membrane using a water immersion, 1.2NA, 60X objective and used a closed-loop nano-positioner to position the nanopore at the confocal spot. Interestingly, X-Y scanning of the sample while registering the ion current passing through the pore, revealed a sharp increase in the open pore current (i_o) when the laser spot overlapped with the nanopore position. This opto-electrical effect is due to light-induced surface charging of the SiN_x membrane, and is discussed in more detail in Section 3. Importantly, it enables fine alignment of laser spot with the nanopore, to sub-wavelength precision.

In the confocal setup described by Di Fiori and coworkers, the emitted light was focused onto a 100 μ m pinhole, and then spectrally split, using a 640 nm dichroic mirror, onto two APDs, for two-color emission detection ('green' and 'red'). For data acquisition, the digital photon streams were fed to multi-channel high-speed counters, and the analog ion current signal was digitized by an A/D card. In order to allow synchronization between the optical and electrical signals, the two cards shared the same 250 KHz sampling clock via a hardware connection, and where fully controlled by a custom program.

3. Background noise suppression strategies

The TIRF and confocal methods described above can suppress background light originating from the bulk or out of focus regions of the sample. They, however, fail to suppress background light emitted by the membrane itself, resulting from scattering, photoluminescence, or even weak fluorescence. This source of background is not negligible and was the focus of a few studies which aimed to minimize it.

The first approach involved modification of the SiN_x surface using atomic layer deposition (ALD) of various oxides [42]. dela Torre and coworkers showed that focused ion beam (FIB) fabricated nanopores and nanopore arrays in SiN_x can be coated with a TiO₂ layer via ALD [31]. The coating served a dual purpose: first, it reduced the nanopore size from roughly 25 nm down to 8 nm, and second, it decreased the surface photoluminescence. Specifically, the TiO₂ layer exhibited much lower photo-luminescence in the 580-660 nm range, when compared with the bare SiN_x. A proof of principle experiment using immobilized Q dots, showed that the TiO₂-coated membrane exhibits a three-fold reduction in the background noise level compared to a bare SiN_x membrane. They then performed optical detection of 1 kbp DNA molecules bound to streptavidin-coated Quantum dots, using TiO₂-coated 6x6 nanopore arrays. When an external electrical field was applied across the membrane, the Qdots-DNA complexes were randomly drawn to the nanopores. The molecules that were captured in the pore got trapped inside the

1
2
3 nanopore array due to the fact that the diameter of the Qdot was larger than the pore
4 diameter. Upon application of a positive voltage, they observed distinct fluorescence
5 signals in some of the pores, indicating Qdot–DNA conjugate lodging in each of the
6 illuminated pores. Switching off the electric field resulted in disappearance of the
7 fluorescence signal, due to escape of the Qdot–DNA from the pore.
8
9

10
11
12 Sawafta and coworkers utilized the beam of a commercial helium ion microscope
13 (HIM) to achieve controllable reduction of the photoluminescence (PL) of SiN_x membranes
14 and to produce nanopore arrays within the membrane [43]. They report a 20% reduction
15 in membrane background noise level from that measured for its unmodified form. The
16 HIM is characterized by a superior beam shape and imaging capabilities as compared with
17 dual beam FIB systems, allowing the direct fabrication of smaller nanopores, and bypass
18 of the need for additional post-fabrication processes, such as ALD [44]. The HIM has been
19 used to fabricate larger nanopore arrays (20 × 20) with diameters of ~5 nm. Sawafta and
20 coworkers used TIRF microscopy to image translocations of short ssDNA molecules
21 labeled with 3 Cy3 fluorophores; the video was collected while applying 1 V across the
22 membrane (Fig 2). Transient increases in fluorescence at the location of the pores were
23 observed, which could have resulted from translocation of the ssDNA molecules through
24 the pores or from free diffusion of a fluorophore into the focal volume of the microscope.
25 Analysis of the event rate showed that the vast majority of the fluorescence spikes
26 measured in the nanopore array corresponded to translocation events or stochastic
27 interactions with the sensing region. In the future, simultaneous measurement of the
28 optical and electrical signals may provide the key for differentiating between true
29 translocations through the pores and other interactions that do not involve translocation.
30
31
32
33
34
35
36
37
38
39
40
41

42 PL in supported SiN_x films has been extensively studied and characterized [45, 46].
43 However, much less is known about PL behavior in freestanding, ultrathin SiN_x
44 membranes, which are the most-commonly used substrates for solid-state nanopore
45 measurements. Understanding PL properties is a crucial step toward the possibility of low
46 SNR optical measurements in solid-state nanopores. Assad and coworkers investigated
47 the effect of controlled focused e-beam irradiation on the optical properties of nanopores
48 made in SiN_x membranes [47]. They illuminated ultrathin SiN_x membranes, immersed in a
49 1M KCl buffer, using blue (488 nm), green (532 nm) and red (640 nm) lasers and measured
50 the emitted PL spectra with a spectrometer. Their results showed that, unlike the red laser
51 that induced low PL, the blue and green excitations produced a broad PL emission band,
52 which substantially overlapped with the emission spectra of common high brightness
53 fluorophores and substantially reduced the SNR (Fig 3a). This can explain why the
54 excitation was restricted to red laser excitation and far-red dyes in all previous optical
55
56
57
58
59
60

1
2
3 experiments performed using nanopores [16]. The group then repeated the
4 measurements at three different regions on the same silicon nitride membrane: a thick
5 region (60 nm), a thin region (15 nm) and a thin region after an exposure to a high e-beam
6 dose, which resulted in nanopore formation (Fig 3b). The shapes of the three spectra
7 measured for the three regions were mostly similar, however, membrane thinning led to a
8 reduction in PL. Electron beam irradiation resulted in an additional reduction by a factor of
9 2, with respect to the unexposed 15 nm-thick area. These results propose two factors
10 underlying reduced PL: thinning down of the silicon nitride and its exposure to a high-
11 dose electron beam.
12
13
14
15
16
17

18
19 In order to understand the mechanism through which e-beam exposure affects the
20 PL intensity and spectra, they compared six thin (15 nm-thick) regions on the same SiN_x
21 membrane that had been irradiated with different e-beam doses. Upon excitation with a
22 488 nm laser, the PL intensity dropped from an initial level of 670 ± 30 counts per
23 millisecond per milliwatt (Cpms/mW) with no e-beam dose, to less than 330 ± 14
24 Cpms/mW when the e-beam dose reached 56×10^6 electron/nm², yet remained roughly
25 stagnant for even larger e-beam dosages. The obtained data fit nicely to an exponential
26 function with an offset baseline, which indicates that there is an additional factor aside
27 from e-beam irradiation controlling the membrane PL. Exposure of thin and thick
28 membrane regions to e-beam for an extended period of time, resulted in similar PL levels,
29 which implies that this PL contribution does not arise from the bulk material [48, 49].
30 Following the observations presented above, Assad et al suggested that highly localized
31 e-beam irradiation of SiN_x during the drilling process of solid-state nanopores induces
32 substantial alterations to the membrane's material properties, resulting in a measurable
33 reduction of the PL intensity and in a blue shift of its spectrum [47].
34
35
36
37
38
39
40
41
42
43
44

45 **iii. Optical detection in solid-state nanopores with Ca²⁺-activated dyes**

46
47 Ca²⁺-activated dyes are organic molecules that become fluorescent upon binding to
48 Ca²⁺ ions [50]. They are commonly used in neuroscience research to monitor neural activity
49 and Ca²⁺ signaling. In nanopore experiments, Ca²⁺-activated dyes can serve as an indicator
50 of the local Ca²⁺ ions concentration near the pore, thus substituting direct ion
51 measurement using the AgCl⁻ electrodes with optical signals. This offers a number of
52 potential benefits towards label-free sensing of analytes in nanopores. First, such dyes can
53 be used to detect the simultaneous ion current flow through multiple pores, without the
54 need to equip each and every pore with its own set of electrode that must be electrically
55 isolated from one another. Second, due to the nature of the chemical gradient of ions
56
57
58
59
60

1
2
3 near the pore, the optical signals are localized to the pore region, and are less affected by
4 ion concentration fluctuations at distances from the pore, as compared to the electrical
5 probes. In principle, this may lead to superior noise characteristics.
6
7

8
9 Heron and co-workers used Ca^{2+} -activated dyes in protein nanopores to probe the
10 stochastic on/off binding kinetics of cyclodextrin to the alpha hemolysin pore by
11 monitoring the fluorescent signal arising from each pore [51]. More recently, two groups
12 independently presented the ability to use Ca^{2+} -activated dyes for optic detection of
13 unlabeled DNA molecules in solid-state nanopores [52, 53], employing higher bandwidth
14 measurements than the previous study. The principle behind the method is to create a
15 Ca^{2+} ion gradient across the pore by injecting high Ca^{2+} concentration in the lower
16 chamber (*trans*) and no calcium in the upper chamber (*cis*). Utilizing numerical simulations,
17 Anderson and co-workers showed that the Ca^{2+} ion distribution around the nanopore can
18 be finely tuned within the pore vicinity by varying the voltage or the Ca^{2+} bulk
19 concentration [53, 54]. Under these conditions, the addition of low concentrations of a
20 Ca^{2+} indicator dye to the *cis* side results in a highly localized and voltage-tunable
21 fluorescent spot immediately outside the nanopore. When a DNA molecule translocates
22 through the pore, it partially blocks the Ca^{2+} flow through the pore, thereby creating an
23 immediate drop in the Ca^{2+} flow and a corresponding drop in the optical signal (Fig 4).
24
25
26
27
28
29
30
31
32

33
34 Both groups presented the ability to use this method for simultaneous detection of
35 DNA translocation events through multiple pores. Ivankin and co-workers employed epi-
36 illumination for the excitation of the Ca^{2+} -activated dyes and an EM-CCD camera for
37 fluorescence detection. They translocated ~150 nt-long ssDNA molecules through three
38 nanopores (2 nm diameter) and simultaneously detected events occurring through the
39 pores (Fig 4d). These authors observed substantial photo-bleaching rate, presumably due
40 to the use of epi-fluorescence illumination, and employed a constant flow of fresh dyes.
41 Anderson and co-workers used TIRF illumination, which permitted the use of much lower
42 laser excitation per unit area, while allowing a somewhat faster frame rate capture. They
43 demonstrated the feasibility of multipore imaging on a 3×3 nanopore array (4 nm
44 diameter). Out of the nine nanopores simultaneously probed in this measurement, four
45 displayed DNA translocation events (8 kbp), one became partially blocked after 20
46 seconds, and the other pores remained open.
47
48
49
50
51
52
53
54

55
56 In addition to the TIRF measurements, Anderson and co-workers developed a
57 method to couple the ionic current to photon-by-photon counting of the fluorescent
58 signal emanating from the Ca^{2+} -sensitive dyes and demonstrated label-free optical
59 detection of biopolymer translocation through solid-state nanopores using confocal
60 microscopy [53]. This provided for higher photon count rates while utilizing pure digital

1
2
3
4
5
6
7
8
9
10
11
12
13
14
15
16
17
18
19
20
21
22
23
24
25
26
27
28
29
30
31
32
33
34
35
36
37
38
39
40
41
42
43
44
45
46
47
48
49
50
51
52
53
54
55
56
57
58
59
60

photon counting. They illuminated the nanopore with a focused laser beam, counted individual emitted photons, using APDs, and simultaneously recorded both electrical and optical open pore currents. In order to compare the electrical and optical noise characteristics, they estimated the power spectra for both signals (Fig 5a,b). The resulting electrical spectrum displayed the typical noise characteristics discussed above. In contrast, the corresponding optical spectrum was virtually flat from 5 Hz to 100 kHz, and specifically no spurious noise was observed. Anderson et al suggested that the observed difference in the noise profile stems from the fact that, unlike the electrical signal, which is measured using electrodes positioned hundreds of micrometers from the pore, the optical signal is generated in the immediate vicinity of the pore, thus involving only local sources of noise (i.e., mainly thermal noise and shot noise). Furthermore, photon arrivals are an inherently digital stream of information, whereas the electrical ion current is an analog signal, subject to sampling error and noise. They further measured and calculated the SNR for the APD counts for three average fluorescence emission intensities (1.3, 4.0, and 9.8 Mcps) and demonstrated substantial growth of the SNR with the average count rate (which can be tuned via the activated fluorophore concentration and excitation intensity) (Fig 5c). Further improvement in the emission count rates will potentially allow researchers to obtain even higher bandwidths than those available today in typical electrical nanopore measurements.

iv. Light-driven manipulation of analytes in solid-state nanopores

1. Controlling the analytes' translocation speed:

Both the electrical and optical signals associated with nanopore sensors are constrained by their corresponding noise levels and the underlying noise spectra. To understand the various trade-offs associated with the technique, it is constructive to define the signal-to-noise ratio (SNR) as:

$$(1) \quad SNR(BW) = \frac{\Delta i}{i_{RMS}(BW)}$$

where Δi is the minimal signal (electrical or optical) amplitude required to make a confident call between two states, and i_{RMS} is the bandwidth (BW)-dependent root mean square (rms) noise level. A confident nanopore measurement is only possible when $SNR(BW) > \varepsilon$, where ε is a number greater than unity. For example, in a nanopore sequencing application, Δi would be the smallest ion current or photon count required to discriminate between the two closest levels associated with two different nucleotides, and i_{RMS} is the calculated rms value of the mean signal level at the bandwidth corresponding to

1
2
3 the same measurement. Importantly, as the bandwidth is increased, the i_{RMS} also
4 increases, while the SNR is reduced. Generally, in single-molecule measurements,
5 particularly in nanopore measurements, it is crucial to make the distinction between the
6 instrument bandwidth BW_I and the measurement bandwidth BW_M . The instrument
7 bandwidth simply reflects the maximal frequency that can be measured by the
8 instrumentation being used before it is attenuated by its internal components. In contrast,
9 the measurement bandwidth is an application-specific parameter defined by the inverse of
10 the minimum amount of time that the signal Δi is integrated. For example, if a DNA
11 strand translocates through the nanopore at a maximal velocity v_{max} and the base-to-base
12 distance in the DNA is a , $BW_M = v_{max}/a$. Clearly, two conditions must be met to obtain a
13 reliable measurement. First, $BW_M < BW_I$, otherwise the obtained signal will be biased by
14 the instrumentation. Second, $SNR(BW_M) > \varepsilon$ to ensure a reliable readout not masked by
15 noise. Therefore, the ability to control and manipulate v_{max} , with subsequent control of
16 the measurement bandwidth, in a way that does not impact the signal (Δi), is of pivotal
17 importance in nanopore sensing.
18
19

20
21
22 One way by which v_{max} can be controlled is by coupling a molecular ratcheting
23 enzyme to the nanopore (for example a DNA polymerase), to regulate the speed of the
24 DNA strand translocation through the nanopore [55]. This idea was successfully adopted
25 to develop protein pore-based DNA sequencing methods. There are, however, limitations
26 on the use of molecular motors as means to regulate strand translocation velocity, which
27 motivated the development of purely physical approaches for controlling v_{max} . Among
28 the various approaches that were proposed for controlling v_{max} , we focus on those which
29 take advantage of light-induced phenomena. Specifically, theoretical studies showed that
30 a controlled electro-osmotic flow in the direction opposing the DNA translocation, could
31 be an efficient and general means of regulating v_{max} .
32
33

34
35
36 Recently, Di Fiori and coworkers showed that a low-power visible laser beam can be
37 used to directly enhance the surface charge of a solid-state nanopore. This, in turn,
38 resulted in modulation of the associated electro-osmotic flow, which allowed them to
39 control the translocation speed of DNA as well as protein molecules through the
40 nanopore [41]. In this work, a low-power green laser (532 nm) was focused, using confocal
41 microscopy, on a silicon nitride membrane containing a single nanopore. As the
42 membrane was scanned with the laser, a substantial increase in the open pore current was
43 observed once the laser spot overlapped with the nanopore location (Fig 6). Di Fiori *et al.*
44 reported a linear dependence of the change in the pore current at varying laser intensities
45 (dI/dP), on nanopore diameter. This observation indicated that the photoconductance-
46 induced charge enhancement is a surface rather than a volumetric phenomenon. They
47
48
49
50
51
52
53
54
55
56
57
58
59
60

1
2
3 hypothesized that the laser illumination on the nanopore creates an increased surface
4 charge density on the nanopore walls. The surface charges induce a diffuse double layer
5 containing an excess of oppositely charged ions, of a thickness comparable to the Debye
6 screening length k^{-1} . The electrical double layer creates a local imbalance of counter ions
7 within k^{-1} , which drags water molecules with its motion, creating an electroosmotic flow
8 (EOF) that, in turn, results in an increase in the open pore current [56].
9

10
11
12
13 Furthermore, the translocation speed of the biopolymers passing through the pore
14 was dramatically reduced when the laser was focused on the pore. This phenomenon is in
15 line with light-induced surface charging and was explained by the increase in the EOF in a
16 direction opposite that of the DNA velocity in the pore. Thus, the laser light can be used
17 to dynamically modulate the DNA translocation speed and hence, the translocation time
18 of the DNA.
19
20
21
22

23
24 Further insight into the photoconductive effect was obtained by a simple model
25 constructed to quantify this phenomenon. The ability of the nanopore surface to acquire
26 charge when illuminated by the laser light, was defined empirically as the photoreactivity,
27 γ (in units of $C/m^2 W$). For sufficiently low laser power, the surface charge density (σ) is
28 assumed to grow linearly with the laser intensity (P) such that: $\sigma = \gamma P$. The reactivity, γ ,
29 is a specific property of each nanopore and depends on its fabrication process.
30 Importantly, γ can be directly determined for each nanopore from the dependence of the
31 open pore current on the laser intensity $i_o(P)$. Translocation experiments using different
32 DNA lengths and different nanopore diameters were all shown to collapse on a single
33 universal curve describing the retardation factor (the magnitude of slowing down upon
34 exposure to light with respect to the no- light conditions) as a function of the nanopore
35 surface charge density calculated using each pore's photoreactivity value.
36
37
38
39
40
41
42
43

44
45 Di Fiori's results show that the DNA and protein translocation speed through a
46 photoreactive nanopore, can be controlled by either the laser intensity or by the pore
47 photoreactivity (Fig 7). The latter was found to directly correlate with the electron beam
48 dosage: pores exposed to a high electron beam dose had much higher photoreactivity in
49 comparison to those that were drilled with a low electron beam dose. It was proposed
50 that the high dose of electrons reduces the N/Si ratio around the pore and when this ratio
51 is sufficiently low, the visible light can excite electrons from the ground state across the
52 bandgap, trapping them in Si dangling bonds [57, 58]. Eventually, trapped electrons
53 recombine with holes, but a high density of arriving photons can maintain a steady state
54 of negatively charged Si dangling bonds, creating a net surface charge density.
55
56
57
58
59
60

2. Conductivity manipulation:

Manipulation of the ionic conduction in solid-state nanopores can be achieved by variation in the local temperature. In 2005, Keyser et al. showed that the temperature of the liquid in a solid-state device can be increased using a focused high-power infrared laser beam [59]. They scanned the pore, measured the ionic current, and calculated the local temperature by means of the linear temperature dependence of KCl conductivity. However, due to the low absorption coefficient of the aqueous buffer medium, this technique was suitable only for high intensity lasers (a few Watts).

Recently, Jonsson et al presented an improved approach to profiling low-intensity optical field distribution at subdiffraction-limited resolutions [60]. In this study, a single plasmonic gold bowtie nanoantenna was fabricated on top of a thin silicon nitride membrane and a 10 nm nanopore was drilled at the center of the structure (Fig 8). Finite difference time domain (FDTD) simulations were used to guide the design of the bowtie antennas so that their plasmon resonance matched the near IR laser wavelength (785 nm) when excited with light polarized along the long side of the structure. Each bowtie consisted of two equilateral gold triangles, separated by a 10 nm gap, with a thickness of 30 nm and a length of 60 nm from the tip to the opposite flat side of the triangle.

The nanoantenna can be used to focus an electromagnetic field to the sub-diffraction gap region between the two gold triangles, where the optical field intensity is amplified. The plasmonic antenna acted like a nanodetector that converts optical intensity variations into temperature variations that, in return, change the measured nanopore's ionic conductance (G), according to (in KCl solution):

$$(2) \quad G = \left(\frac{4h}{\pi d^2} + \frac{1}{d} \right) \mu c_{KCl} e$$

$$\mu = \mu_K + \mu_{Cl} \propto 1/\eta$$

where h is the membrane effective thickness, d is the pore diameter, μ is the total ion mobilities, which is inversely dependent on the buffer viscosity η , c_{KCl} is the ion molar concentration and e is the elementary charge. Aqueous buffer viscosity empirically inversely depends, to a good approximation, on the temperature, expressed in degrees Celsius [61]. Thus, we can see that: $G \propto T(^{\circ}C)$. Unlike the approach presented by Keyser et al., which was based on light absorption by the buffer, this method is based on local light absorption by the nanopore itself, through excitation of plasmons in the nanoantenna. In consequence, a greater heating can be obtained and signals are nearly 2 orders of magnitude higher compared to those obtained using direct heating.

1
2
3
4 In a follow up study, Nicoli and coworkers demonstrated label-free detection of
5 DNA molecules using the same solid-state plasmonic nanopores, and explored the effects
6 of plasmon excitation on the translocation parameters [62]. They added 48.5 kilo basepair
7 dsDNA molecules in 1M KCl buffer to one of the chambers, applied a 100 mV potential
8 across the membrane and measured the ionic current with and without plasmonic
9 excitation. Their results showed that both the open pore current and the conductance
10 blockade increased upon laser excitation. However, the relative conductance blockades
11 ($\Delta G/G$) decreased slightly with increasing laser power, likely due to other effects beside
12 heating, such as light-induced changes in the surface charge density at the pore wall [41].
13 Interestingly, they did not observe significant changes in the translocation time upon
14 plasmonic excitation. This may result from the fact that plasmonic heating is a highly local
15 phenomenon, or from a balance between the competing effects of increased temperature
16 and light-induced surface charging of the nanopore. Similar results were obtained in 2 M
17 LiCl buffer.

26 3. Events rate manipulation:

27
28
29 In addition to conductance manipulations, Nicoli and coworkers showed that the
30 plasmonic system could be used as a tool for controllable and reversible manipulation of
31 the events rate in LiCl buffers. In the experiments performed, the event rate in 2M LiCl
32 buffer was measured under different laser intensities. The 2M LiCl buffer has a similar
33 conductivity as 1M KCL, with the ability to provide for significantly lower translocation
34 velocities but at the expense of low event rates. Upon longitudinal excitation with a 2 mW
35 laser, they observed an order of magnitude enhancement in the event rate excitation. A
36 ~30% of the enhancement in longitudinal mode was also observed in the transverse
37 mode. The measurements were repeated using different plasmonic nanopore chips and
38 polarizations and the relative increase in open pore current under laser illumination ($\delta I/I$,
39 where δI is the difference between the open pore current with and without laser
40 illumination) was calculated. Interestingly, all the results collapsed to display a linear
41 dependence of the event rate on $\delta I/I$. This result, in addition to the insensitivity to the
42 other experimental conditions (specifically to polarization), indicates that the event rate
43 enhancement is related to the strong and local thermal gradients caused by plasmon-
44 induced heating. To explain this, Nicoli et al. proposed that negative thermophoresis (in
45 which molecules move from cold to warm regions) facilitates capture of the DNA
46 molecules by moving them toward the warmer nanopore [63, 64]. Unlike LiCl, which is
47 known to result in negative thermophoresis, KCl induces positive thermophoresis and,
48 indeed, the rate enhancement effect was not observed for DNA translocations in KCl
49 buffer.
50
51
52
53
54
55
56
57
58
59
60

v. Applications – Next-generation DNA sequencing and beyond

The high demand for low-cost and ultra-fast sequencing technologies has driven the development of multiple, novel single-molecule methods [65]. Among them, nanopore based DNA sequencing is widely considered to be a promising next-generation sequencing platform [11, 66]. As of the writing of this paper, protein pores (i.e., MspA) have already been shown to effectively sequence DNA strands [12, 14, 55]. This was achieved by reducing the translocation speed of the DNA strands by coupling them to ratcheting enzymes. Two primary challenges for the method still remain: First, improving the base calling accuracy and its ability to read any arbitrary sequence including long repeats. Second, realizing a drastic boost in the overall throughput of nanopore sequencing by simultaneous readout from hundreds if not thousands of nanopore. These may potentially be addressed by employing optical-based nanopore techniques with high-density nanopore arrays [31, 43].

Soni et al. first introduced an optical-based nanopore sequencing approach that involves two steps [17]. First, a sample preparation in which the DNA is converted to an expanded form, followed by hybridization of fluorescently-labeled probes to each expanded base. Second, the fluorescent markers are optically detected, using an array of nanopores and TIRF illumination (Fig 9). The main advantage of the method is that it simplifies the readout procedure to involve only four different-colored fluorophores. In contrast, the current electrical-based nanopore sequencing method involves a readout of 3 (or 4) nucleotides groups, which theoretically, require discrimination among $4^3 = 64$ different current levels, although sophisticated algorithms can be used to reduce this number by exploiting the fact that DNA is ratcheted through the pore in discrete single-nucleotides steps and that each base is read 3 (or 4) times in a different sequence context [67, 68]. The optical approach in contrast, does not involve ratcheting enzymes and thus can theoretically, achieve a higher strand loading efficiency and higher sequencing speed.

These advantages, however, come at the price of an elaborate DNA preparation step, in which each of the four different nucleotides in the DNA strand is substituted with its own unique code oligonucleotide (typically ~15 nucleotide long). The substitution (or "DNA conversion") process involves cyclic ligations of the correct code oligonucleotide and digestion of the original bases. This off-line process can be simultaneously performed to a vast number of DNA molecules and does not require enzyme immobilization or an amplification step. After converting the DNA molecules, four different molecular beacons complementary to the four possible oligonucleotide codes, are specifically hybridized to the converted DNA. Each of the four beacons contains a different color fluorophore on its 5' end and a quencher on its 3' end. The broad-spectrum quencher molecule quenches

1
2
3 both fluorophores and the four different color fluorophores make it possible to distinguish
4 between them.
5
6

7 The converted DNA strands and hybridized beacons are electrophoretically
8 threaded through an array of nanopores, designed to bear a diameter that allows only one
9 strand to translocate through it. The pores are illuminated with a laser source in TIR mode
10 and optically monitored using EMCCD. When the DNA molecule enters the pore, the
11 marked beacons are stripped off one at the time, creating a distinct burst of fluorescence.
12 Each released beacon is automatically closed, quenching its own fluorescence while
13 diffusing away from the vicinity of the pore (Fig 9, lower panel). The stripping process
14 slows down the translocation speed of the DNA to approximately a few ms per unzipping
15 event. This unzipping time can be tuned by the voltage applied.
16
17
18
19
20
21

22 McNally and coworkers performed proof of concept experiments to validate this
23 new sequencing method [16]. In order to use larger pores than the ones needed for the
24 unzipping process (~ 2 nm), they covalently attached a "bulky" group (e.g., a protein or a
25 nanoparticle) to the molecular beacons, which effectively increased the molecular cross
26 section of the complex to 5-7 nm, enabling use of 3-5 nm pores. In this study, each of the
27 four possible nucleotides was represented by two successive beacons (or "bits"), allowing
28 for use of two colors only. To test the ability to observe the 2 bit signal, they prepared
29 two samples: a 1 bit sample in which they attached an avidin (4X5X6 nm) to a biotinylated
30 molecular beacon containing a fluorophore-quencher pair, in addition to a similar beacon
31 without a fluorophore, both hybridized to a target ssDNA, and a 2 bit sample with a
32 similar complex but with two beacons containing a fluorophore-quencher pair. The optical
33 signals clearly showed one and two-photon bursts for the 1-bit and 2-bit samples,
34 respectively.
35
36
37
38
39
40
41
42
43

44 Next, they performed two-color unzipping experiments with two high quantum yield
45 fluorophores A647 (ATTO647N) and A680 (ATTO680), simultaneously excited by the same
46 red laser. The optical emission was split into two channels using a dichroic mirror and
47 simultaneously imaged by a single EM-CCD camera. Due to the overlap between the
48 emission spectra of the two fluorophores, they performed calibration experiments using
49 1-bit complexes labeled either with A647 or A680. The ratio of the fluorescent intensities
50 in Channel 2 versus Channel 1 was 0.2 ± 0.06 for the A647 sample and 0.4 ± 0.05 for the
51 A680 sample. The ratios for the accumulation of all the events were 0.2 and 0.4 for the
52 A647- and A680-labeled sample, respectively. The control measurements showed that the
53 color ratio can be used in order to determine the identity of individual fluorophores. The
54 error in the determination of each of the two fluorophores was calculated from the
55 overlap area between the distributions, yielding <9% for the A647 and <13% for A680.
56
57
58
59
60

1
2
3 Using the calibration results, they tested their ability to discriminate between the 2
4 bit combinations representing the four different bases (Fig 10). Analysis of ~2000 events
5 in which two distinct photon bursts were detected, revealed a bimodal distribution of R
6 with two modes at 0.21 ± 0.05 and 0.41 ± 0.06 , in agreement with the calibration results.
7 Photon bursts with $R < 0.3$ were classified as 0 and those with $R > 0.3$ were classified as 1.
8 Finally, they demonstrated multipore reading of the photon bursts using an array of 3
9 nanopores.
10

11
12
13
14
15 Although this method provides a new approach for high-throughput DNA
16 sequencing, the SNR and error in barcode determination due to spectra overlap must be
17 further improved. One of the possible ways in which the barcoding error can be reduced
18 is by use of fluorophores with less overlap in their emission spectra. This could be
19 achieved by simultaneously illuminating the nanopore with multiple laser lines. Using this
20 idea, Assad and coworkers have been able to extend the range of usable fluorophores, by
21 exploiting low PL nanopores fabricated in a thinned down silicon nitride membrane. Under
22 these conditions, it was possible to detect DNA labeled with individual green-yellow (5-
23 carboxytetramethylrhodamine, TMR) and red (Atto647) fluorophores having $\lambda_{EM} = 565$ nm
24 and 665 nm, respectively [69]. In this study, DNA barcode constructs consisting of five 16-
25 nucleotide-long, fluorophore-quencher beacons hybridized in a head-to-tail configuration
26 along a template strand were used. Assad and coworkers used two alternative constructs:
27 a single-color barcode (TMR), and a dual-color barcode (TMR and Atto647, at a specific
28 order) simultaneously excited by red and green lasers. They simultaneously recorded the
29 electrical current and the optical current; for the optical signals, they used confocal
30 microscopy and 2 APDs, in a configuration similar to that used by Anderson et al [53]. The
31 optic events showed five discrete photon bursts associated with the unzipping and fast
32 diffusion of the five molecular beacons hybridized to the template DNA molecule (Fig 11).
33 In both signals (using a single-color barcode and a dual-color barcode), the SNR was high,
34 and no photon bursts were observed in between events.
35
36
37
38
39
40
41
42
43
44
45
46
47

48 The ability to use blue and green laser excitations, which was previously impossible
49 due to low SNR, and the new understanding of the nature of PL in SiN_x membranes, may
50 significantly contribute to the improvement of nanopore-based, optical DNA sequencing
51 methods as well as to other future applications.
52
53
54
55

56 vi. Future advancements

57
58 Single-molecule fluorescence sensing has been evolved substantially in the past two
59 decades, opening up new avenues in biomedical research and in biotechnology [70].
60

1
2
3
4
5
6
7
8
9
10
11
12
13
14
15
16
17
18
19
20
21
22
23
24
25
26
27
28
29
30
31
32
33
34
35
36
37
38
39
40
41
42
43
44
45
46
47
48
49
50
51
52
53
54
55
56
57
58
59
60

Single-molecule, optical sensing in solid-state nanopores is a powerful new approach that allows a high-bandwidth and high-throughput detection from multiple nanopores simultaneously. In this review we focused on the strategies employed to advance optical sensing in small nanopores; namely reduction in the background noise either by optical means to eliminate light emitted by nearby objects or by suppression of photoluminescence originated at the membrane itself. We also described two strategies to enhance the localization of the fluorescence signal to the close vicinity of the nanopore, by introducing a steep gradient of Ca_{2+} ions near the pore, or by the use of molecular beacons that can quench fluorescence from all molecules, except the one residing at the pore entrance.

Optical sensing in nanopores complements the electrical sensing in a number of useful ways. For example, multi-color 'bar-coding' of individual molecules can be used to tag specific DNAs and potentially allow precise quantifications of genes or RNA transcripts, at the single-molecule level. Additionally, the photon emission intensity can be coupled to the nanopore ionic conductance by the use of Ca^{2+} activated dyes, permitting a purely digital sensing of the pore conductance which is less obscured by electrical interferences. Moreover, optical sensing in nanopores can be integrated with nano-channels that are used to efficiently deliver long double-stranded DNA or other biopolymers [71]. Therefore, and particularly with further improvements of the optical SNR in solid-state nanopores it is likely that additional sensing applications will be realized. Additionally, other optical approaches, such as Förster Resonance Energy Transfer (FRET) [72, 73], Fluorescence Correlation Spectroscopy (FCS) [74] and super resolution strategies such as Stimulated Emission Depletion (STED) [75, 76] could be used to further enhance the method providing it with superior spatial and temporal resolutions.

Bibliography

1. Wanunu, M., et al., *Electrostatic focusing of unlabelled DNA into nanoscale pores using a salt gradient*. *Nat Nano*, 2010. **5**(2): p. 160-165.
2. Wanunu, M., et al., *DNA Translocation Governed by Interactions with Solid-State Nanopores*. *Biophysical Journal*, 2008. **95**(10): p. 4716-4725.
3. Plesa, C., et al., *Fast translocation of proteins through solid state nanopores*. *Nano Lett*, 2013. **13**(2): p. 658-63.
4. Wanunu, M. and A. Meller, *Single-molecule analysis of nucleic acids and DNA-protein interactions using nanopores*, in *Single-Molecule Techniques: A Laboratory Manual*, P. Selvin and T.J. Ha, Editors. 2008, Cold Spring Harbor Laboratory Press: Cold Spring Harbor, NY. p. 395–420.
5. Dekker, C., *Solid-state nanopores*. *Nature Nanotechnology*, 2007. **2**(4): p. 209-215.
6. Storm, A.J., et al., *Fabrication of solid-state nanopores with single-nanometre precision*. *Nat Mater*, 2003. **2**(8): p. 537-40.
7. McNally, B., M. Wanunu, and A. Meller, *Electromechanical Unzipping of Individual DNA Molecules Using Synthetic Sub-2 nm Pores*. *Nano Letters*, 2008. **8**(10): p. 3418-3422.
8. Kim, M.J., et al., *Rapid Fabrication of Uniformly Sized Nanopores and Nanopore Arrays for Parallel DNA Analysis*. *Advanced Materials*, 2006. **18**(23): p. 3149-3153.
9. Meller, A., *Nanopores: Single-Molecule Sensors of Nucleic Acid-Based Complexes*, in *Advances in Chemical Physics*. 2012, John Wiley & Sons, Inc. p. 251-268.
10. Stoloff, D.H. and M. Wanunu, *Recent trends in nanopores for biotechnology*. *Curr Opin Biotechnol*, 2013. **24**(4): p. 699-704.
11. Branton, D., et al., *The potential and challenges of nanopore sequencing*. *Nature biotechnology*, 2008. **26**(10): p. 1146-53.
12. Clarke, J., et al., *Continuous base identification for single-molecule nanopore DNA sequencing*. *Nat Nanotechnol*, 2009. **4**(4): p. 265-70.
13. Venkatesan, B.M. and R. Bashir, *Nanopore sensors for nucleic acid analysis*. *Nat Nano*, 2011. **6**(10): p. 615-624.
14. Manrao, E.A., et al., *Reading DNA at single-nucleotide resolution with a mutant MspA nanopore and phi29 DNA polymerase*. *Nat Biotechnol*, 2012. **30**(4): p. 349-53.
15. Ayub, M., et al., *Nanopore-based identification of individual nucleotides for direct RNA sequencing*. *Nano Lett*, 2013. **13**(12): p. 6144-50.
16. McNally, B., et al., *Optical recognition of converted DNA nucleotides for single-molecule DNA sequencing using nanopore arrays*. *Nano Lett*, 2010. **10**(6): p. 2237-44.
17. Soni, G.V. and A. Meller, *Progress toward ultrafast DNA sequencing using solid-state nanopores*. *Clinical chemistry*, 2007. **53**(11): p. 1996-2001.
18. Venkatesan, B.M. and R. Bashir, *Solid State Nanopores Sensors for Nucluc Acid Analysis*, in *Nanopores, Sensing and Fundamental Biological Interactions*. 2011, Springer.
19. Butler, T.Z., J.H. Gundlach, and M.A. Troll, *Determination of RNA Orientation during Translocation through a Biological Nanopore*. *Biophysical Journal*, 2006. **90**(1): p. 190-199.
20. Wanunu, M., et al., *Nanopore analysis of individual RNA/antibiotic complexes*. *ACS Nano*, 2011. **5**(12): p. 9345-53.
21. Wanunu, M., et al., *Rapid electronic detection of probe-specific microRNAs using thin nanopore sensors*. *Nat Nano*, 2010. **5**(11): p. 807-814.
22. Firnkes, M., et al., *Electrically facilitated translocations of proteins through silicon nitride nanopores: conjoint and competitive action of diffusion, electrophoresis, and electroosmosis*. *Nano Lett*, 2010. **10**(6): p. 2162-7.
23. Kowalczyk, S.W., A.R. Hall, and C. Dekker, *Detection of local protein structures along DNA using solid-state nanopores*. *Nano Lett*, 2010. **10**(1): p. 324-8.

- 1
 - 2
 - 3
 - 4
 - 5
 - 6
 - 7
 - 8
 - 9
 - 10
 - 11
 - 12
 - 13
 - 14
 - 15
 - 16
 - 17
 - 18
 - 19
 - 20
 - 21
 - 22
 - 23
 - 24
 - 25
 - 26
 - 27
 - 28
 - 29
 - 30
 - 31
 - 32
 - 33
 - 34
 - 35
 - 36
 - 37
 - 38
 - 39
 - 40
 - 41
 - 42
 - 43
 - 44
 - 45
 - 46
 - 47
 - 48
 - 49
 - 50
 - 51
 - 52
 - 53
 - 54
 - 55
 - 56
 - 57
 - 58
 - 59
 - 60
24. Singer, A., et al., *Electronic barcoding of a viral gene at the single-molecule level*. Nano Lett, 2012. **12**(3): p. 1722-8.
25. Singer, A., et al., *Nanopore based sequence specific detection of duplex DNA for genomic profiling*. Nano Lett, 2010. **10**(2): p. 738-42.
26. Rosenstein, J.K., et al., *Integrated nanopore sensing platform with sub-microsecond temporal resolution*. Nat Methods, 2012. **9**(5): p. 487-92.
27. Uram, J.D., K. Ke, and M. Mayer, *Noise and bandwidth of current recordings from submicrometer pores and nanopores*. ACS Nano, 2008. **2**(5): p. 857-72.
28. Smeets, R.M., et al., *Noise in solid-state nanopores*. Proc Natl Acad Sci U S A, 2008. **105**(2): p. 417-21.
29. Smeets, R.M., N.H. Dekker, and C. Dekker, *Low-frequency noise in solid-state nanopores*. Nanotechnology, 2009. **20**(9): p. 095501.
30. Tabard-Cossa, V., et al., *Noise analysis and reduction in solid-state nanopores*. Nanotechnology, 2007. **18**(30): p. -.
31. dela Torre, R., et al., *Fabrication and characterization of solid-state nanopore arrays for high-throughput DNA sequencing*. Nanotechnology, 2012. **23**(38): p. 385308.
32. Traversi, F., et al., *Detecting the translocation of DNA through a nanopore using graphene nanoribbons*. Nat Nanotechnol, 2013. **8**(12): p. 939-45.
33. Schneider, G.F., et al., *DNA translocation through graphene nanopores*. Nano Lett, 2010. **10**(8): p. 3163-7.
34. Merchant, C.A., et al., *DNA translocation through graphene nanopores*. Nano Lett, 2010. **10**(8): p. 2915-21.
35. Garaj, S., et al., *Graphene as a subnanometre trans-electrode membrane*. Nature, 2010. **467**(7312): p. 190-3.
36. Venkatesan, B.M., et al., *Stacked graphene-Al₂O₃ nanopore sensors for sensitive detection of DNA and DNA-protein complexes*. ACS Nano, 2012. **6**(1): p. 441-50.
37. Axelrod, D., *Total internal reflection fluorescence microscopy in cell biology*. Traffic, 2001. **2**(11): p. 764-74.
38. Andersen, K.N., et al., *Annealing and deposition effects of the chemical composition of silicon-rich nitride*. Applied Surface Science, 2005. **243**(1-4): p. 401-408.
39. Soni, G.V., et al., *Synchronous optical and electrical detection of biomolecules traversing through solid-state nanopores*. Rev Sci Instrum, 2010. **81**(1): p. 014301.
40. Inoué, S., *Foundations of Confocal Scanned Imaging in Light Microscopy*, in *Handbook Of Biological Confocal Microscopy*, J.B. Pawley, Editor. 2006, Springer US. p. 1-19.
41. Di Fiori, N., et al., *Optoelectronic control of surface charge and translocation dynamics in solid-state nanopores*. Nat Nanotechnol, 2013. **8**(12): p. 946-51.
42. Chen, P., et al., *Atomic Layer Deposition to Fine-Tune the Surface Properties and Diameters of Fabricated Nanopores*. Nano Lett, 2004. **4**(7): p. 1333-1337.
43. Sawafta, F., et al., *Solid-state nanopores and nanopore arrays optimized for optical detection*. Nanoscale, 2014. **6**(12): p. 6991-6.
44. Ward, B.W., J.A. Notte, and N.P. Economou, *Helium ion microscope: A new tool for nanoscale microscopy and metrology*. Journal of Vacuum Science & Technology B, 2006. **24**(6): p. 2871-2874.
45. Park, N.M., et al., *Quantum confinement in amorphous silicon quantum dots embedded in silicon nitride*. Phys Rev Lett, 2001. **86**(7): p. 1355-7.
46. Wang, M., et al., *Photoluminescence of Si-rich silicon nitride: Defect-related states and silicon nanoclusters*. Applied Physics Letters, 2007. **90**(13): p. 131903.
47. Assad, O.N., et al., *Two color DNA barcode detection in photoluminescence suppressed silicon nitride nanopores*. Nano Lett, 2015. **15**(1): p. 745-52.
48. Huang, R., et al., *Strong green-yellow electroluminescence from oxidized amorphous silicon nitride light-emitting devices*. Applied Physics Letters, 2007. **90**(9): p. 093515.

- 1
- 2
- 3
- 4 49. Rui, H., et al., *Oxygen induced strong green light emission from low-temperature grown amorphous silicon nitride films*. Applied Physics Letters, 2006. **89**(22): p. 221120-221120-3.
- 5
- 6 50. Shuai, J. and I. Parker, *Optical single-channel recording by imaging Ca²⁺ flux through individual ion channels: theoretical considerations and limits to resolution*. Cell Calcium, 2005. **37**(4): p. 283-299.
- 7
- 8
- 9 51. Heron, A.J., et al., *Simultaneous measurement of ionic current and fluorescence from single protein pores*. J Am Chem Soc, 2009. **131**(5): p. 1652-3.
- 10
- 11 52. Ivankin, A., et al., *Label-Free Optical Detection of Biomolecular Translocation through Nanopore Arrays*. ACS Nano, 2014. **8**(10): p. 10774-81.
- 12
- 13 53. Anderson, B.N., et al., *Probing solid-state nanopores with light for the detection of unlabeled analytes*. ACS Nano, 2014. **8**(11): p. 11836-45.
- 14
- 15 54. Anderson, B.N., *Enhancing the Temporal and Spatial Resolution of Solid-State Nanopore Single-Molecule Sensors*. 2013, Ph.D. Dissertation, Boston University, Boston, MA.
- 16
- 17 55. Cherf, G.M., et al., *Automated forward and reverse ratcheting of DNA in a nanopore at 5-A precision*. Nat Biotechnol, 2012. **30**(4): p. 344-8.
- 18
- 19 56. Chen, Y., et al., *Electroosmotic flow in nanotubes with high surface charge densities*. Nano Lett, 2008. **8**(1): p. 42-8.
- 20
- 21 57. Howitt, D.G., et al., *The electron beam hole drilling of silicon nitride thin films*. Journal of Applied Physics, 2008. **103**(2): p. 024310.
- 22
- 23 58. Wu, M.Y., et al., *Control of shape and material composition of solid-state nanopores*. Nano Lett, 2009. **9**(1): p. 479-84.
- 24
- 25 59. Keyser, U.F., et al., *Nanopore tomography of a laser focus*. Nano Lett, 2005. **5**(11): p. 2253-6.
- 26
- 27 60. Jonsson, M.P. and C. Dekker, *Plasmonic nanopore for electrical profiling of optical intensity landscapes*. Nano Lett, 2013. **13**(3): p. 1029-33.
- 28
- 29 61. Meller, A. and D. Branton, *Single molecule measurements of DNA transport through a nanopore*. Electrophoresis, 2002. **23**(16): p. 2583-91.
- 30
- 31 62. Nicoli, F., et al., *DNA Translocations through Solid-State Plasmonic Nanopores*. Nano Lett, 2014. **14**(12): p. 6917-25.
- 32
- 33 63. Duhr, S. and D. Braun, *Why molecules move along a temperature gradient*. Proc Natl Acad Sci U S A, 2006. **103**(52): p. 19678-82.
- 34
- 35 64. Putnam, S.A. and D.G. Cahill, *Transport of nanoscale latex spheres in a temperature gradient*. Langmuir, 2005. **21**(12): p. 5317-23.
- 36
- 37 65. Gupta, P.K., *Single-molecule DNA sequencing technologies for future genomics research*. Trends in Biotechnology, 2008. **26**(11): p. 602-611.
- 38
- 39 66. Haque, F., et al., *Solid-State and Biological Nanopore for Real-Time Sensing of Single Chemical and Sequencing of DNA*. Nano Today, 2013. **8**(1): p. 56-74.
- 40
- 41 67. Comer, J. and A. Aksimentiev, *Predicting the DNA Sequence Dependence of Nanopore Ion Current Using Atomic-Resolution Brownian Dynamics*. The Journal of Physical Chemistry C, 2012. **116**(5): p. 3376-3393.
- 42
- 43 68. Timp, W., J. Comer, and A. Aksimentiev, *DNA Base-Calling from a Nanopore Using a Viterbi Algorithm*. Biophysical Journal, 2012. **102**(10): p. L37-L39.
- 44
- 45 69. Assad, O.N., et al., *Two color DNA barcode detection in photoluminescence suppressed silicon nitride nanopores*. Nano Lett, 2014.
- 46
- 47 70. Joo, C., et al., *Advances in single-molecule fluorescence methods for molecular biology*. Annu Rev Biochem, 2008. **77**: p. 51-76.
- 48
- 49 71. Liu, S., et al., *Electro-optical detection of single lambda-DNA*. Chem Commun (Camb), 2015. **51**(11): p. 2084-7.
- 50
- 51 72. Roy, R., S. Hohng, and T. Ha, *A practical guide to single-molecule FRET*. Nat Meth, 2008. **5**(6): p. 507-516.
- 52
- 53 73. Ha, T., *Single-Molecule Fluorescence Resonance Energy Transfer*. Methods, 2001. **25**(1): p. 78-86.
- 54
- 55
- 56
- 57
- 58
- 59
- 60

- 1
 - 2
 - 3
 - 4
 - 5
 - 6
 - 7
 - 8
 - 9
 - 10
 - 11
 - 12
 - 13
 - 14
 - 15
 - 16
 - 17
 - 18
 - 19
 - 20
 - 21
 - 22
 - 23
 - 24
 - 25
 - 26
 - 27
 - 28
 - 29
 - 30
 - 31
 - 32
 - 33
 - 34
 - 35
 - 36
 - 37
 - 38
 - 39
 - 40
 - 41
 - 42
 - 43
 - 44
 - 45
 - 46
 - 47
 - 48
 - 49
 - 50
 - 51
 - 52
 - 53
 - 54
 - 55
 - 56
 - 57
 - 58
 - 59
 - 60
74. Bonnet, O.K.a., *Fluorescence correlation spectroscopy: the technique and its applications*. REPORTS ON PROGRESS IN PHYSICS, 2002. **65**: p. 251–297.
75. Hell, S.W., *Far-field optical nanoscopy*. Science, 2007. **316**(5828): p. 1153-8.
76. Klar, T.A., et al., *Fluorescence microscopy with diffraction resolution barrier broken by stimulated emission*. Proc Natl Acad Sci U S A, 2000. **97**(15): p. 8206-10.

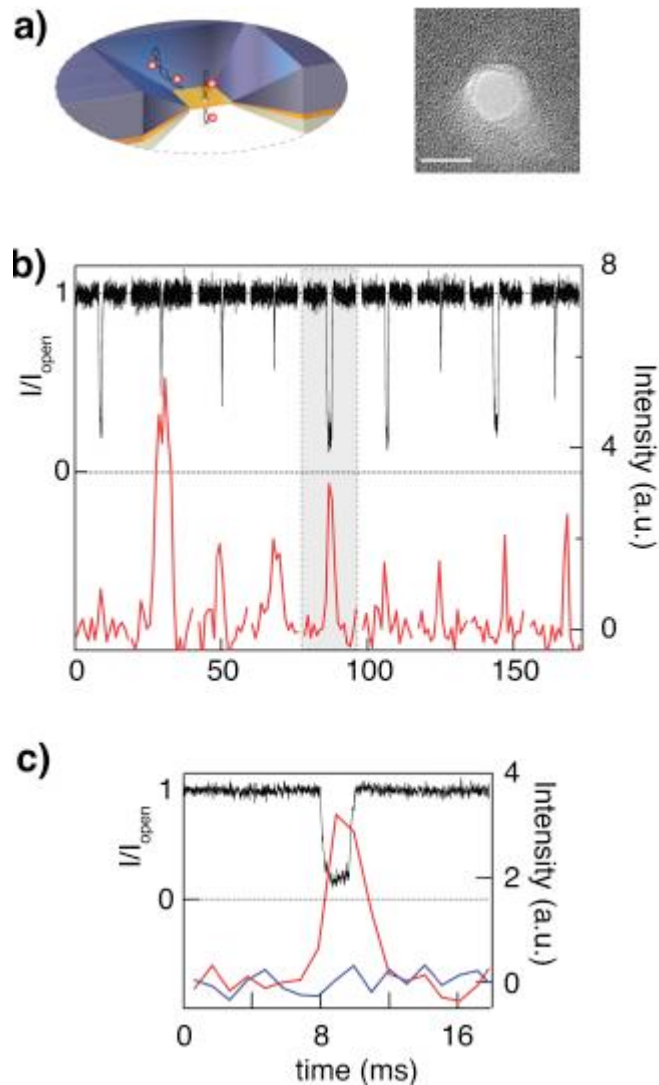


Figure 1 | Synchronous electrical and optical recording of dsDNA translocations through a solid-state nanopore. (a) Schematic illustration of labeled DNA fragments passing through a 4 nm nanopore (TEM image on the right). (b) A typical set of concatenated translocation events measured both optically (red lines) and electrically (black lines). (c) A magnified view of the highlighted event (gray background in b). Reprinted with permission from Soni et al. [39]. Copyright 2010, AIP Publishing LLC.

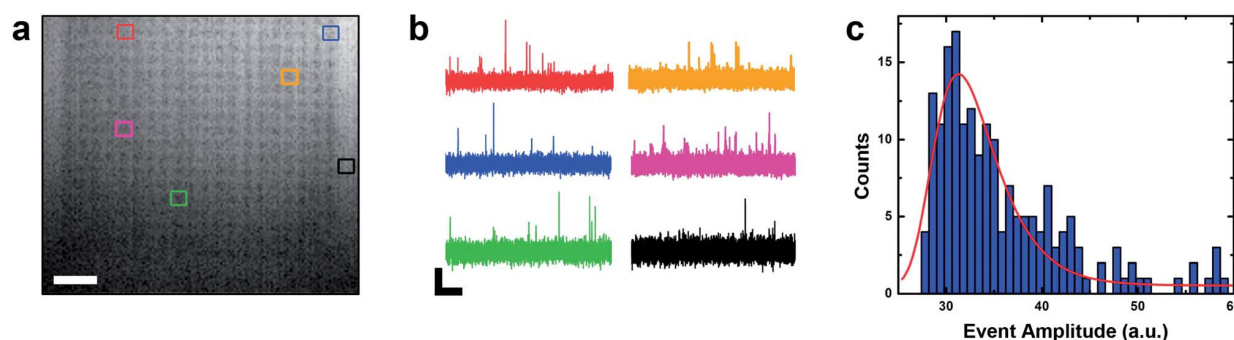


Figure 2 | Parallel optical detection of Cy3 labeled DNA molecules translocating through nanopore array. (a) Fluorescence Image of a 20 \times 20 nanopores array fabricated in a SiN_x membrane. The image is an average of 100 video frames after contrast adjustment. Scale bar is 2.5 μ m. (b) Optical measurements recorded simultaneously from 5 different pores within the array (each outlined in corresponding color) and from a region on the membrane proximal to the array (black lines). Scale bar is 0.5 s (horizontal) and 30 a.u. (vertical). (c) Amplitude histogram of 191 optical events measured at the locations of individual nanopores within the array and a log normal fit to the data (red line). Adapted from Sawafta et al. [43] with permission of The Royal Society of Chemistry.

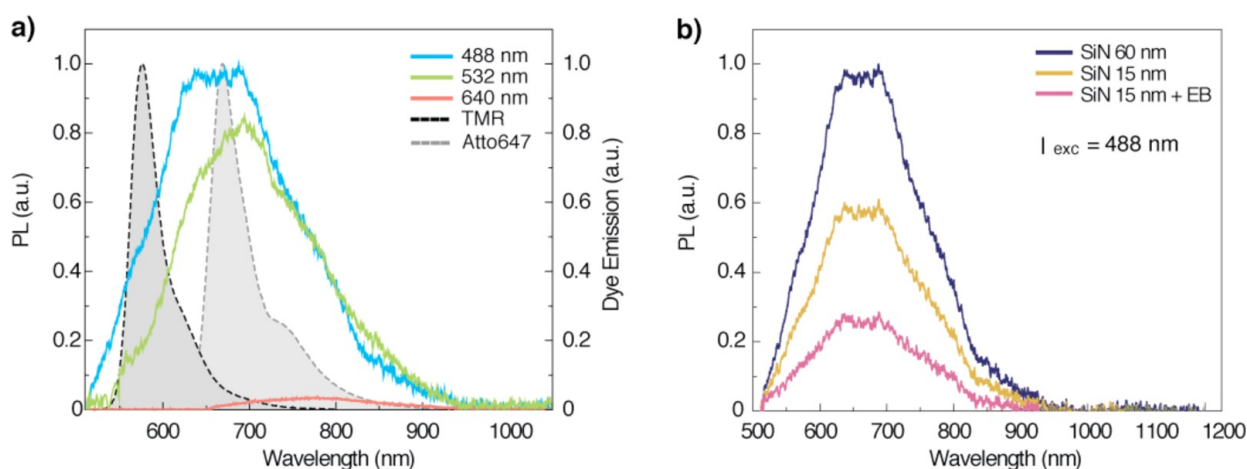


Figure 3 | Photoluminescence spectra of ultrathin SiN_x membranes suspended in 1M KCl buffer. (a) Spectra measured under illumination of blue (488 nm), green (532 nm), or red (640 nm) lasers. Data is normalized by the incoming lasers intensities to permit comparison. Emission spectra of two common single-molecule fluorophores: TMR and Atto647. (b) Spectra measured at three different regions on the same silicon nitride membrane excited by 488 nm laser: a thick region (60 nm) a thin region (15 nm) and a thin region after an exposure to a high e-beam dose, forming a nanopore. Adapted with permission from Assad et al.[47]. Copyright 2014 American Chemical Society.

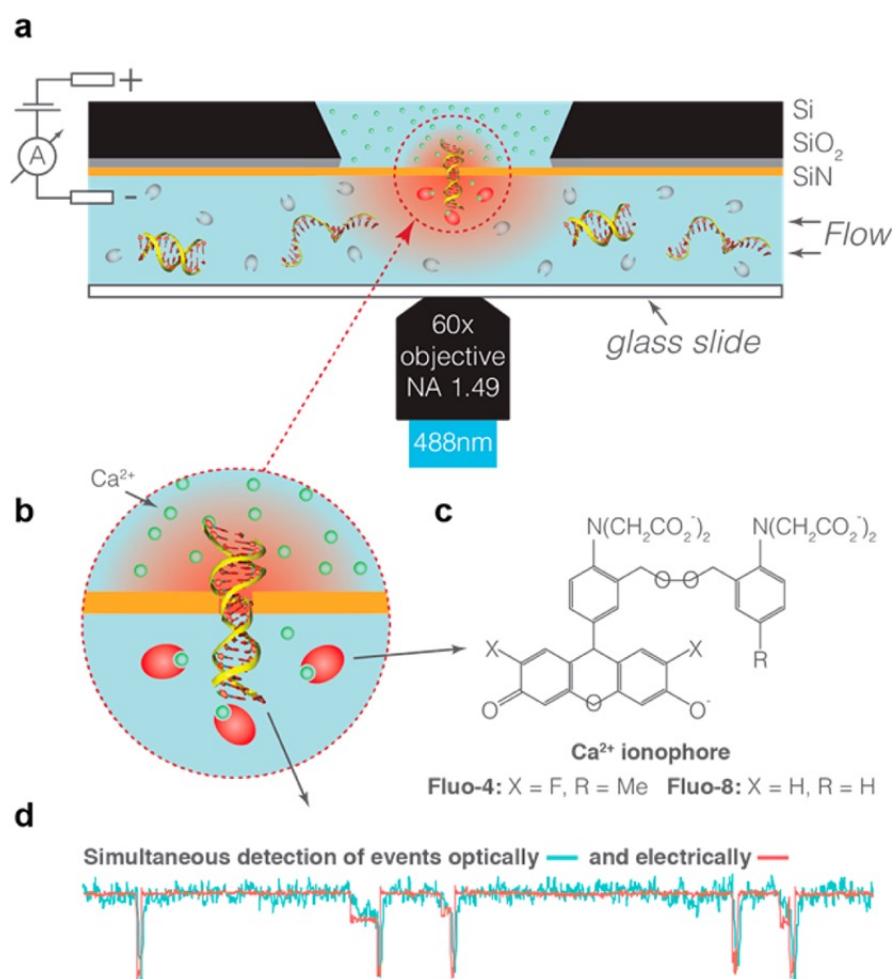


Figure 4 | Chemo optical sensing in solid-state nanopores using Ca²⁺ gradient and calcium activated dyes. (a) Schematic of the measurement set up. The ion current flowing through the pore is probed electrically using Ag/AgCl electrodes and optically using epi illumination for the excitation of the Ca²⁺ indicator dyes and EM-CCD camera for the fluorescence detection. (b) Zoom in on the nanopore area. A gradient of Ca²⁺ ions is created across the pore by using high Ca²⁺ concentration in the upper chamber (*trans*) and no calcium in the bottom chamber (*cis*). The addition of Ca²⁺ indicator dye to the *cis* side results in a highly localized and voltage-tunable fluorescent spot in the vicinity of the pore. (c) The chemical structure of the calcium activated dyes. (d) Simultaneous electrical and optical detection of translocation events. The entry and passage of the biopolymer through the pore results in a drop in the ionic current (red trace) and thus a decrease in the fluorescence intensity (blue trace). Adapted with permission from Ivankin et al. [52]. Copyright 2014 American Chemical Society.

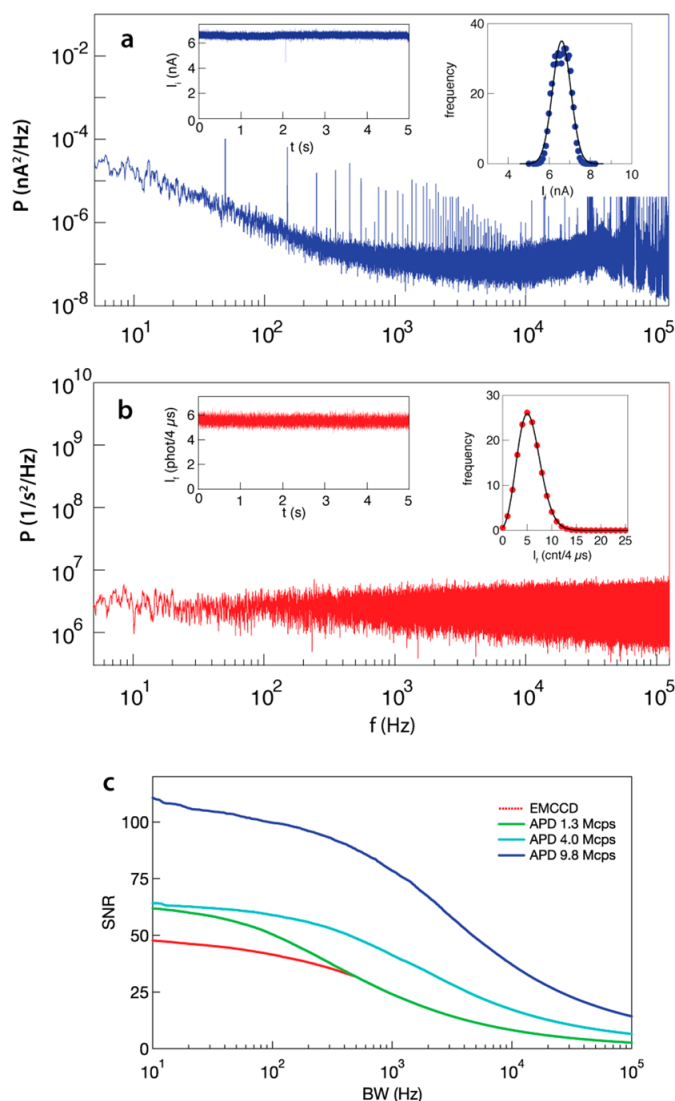


Figure 5 | Electrical and optical noise spectra. (a) The electrical noise exhibits low frequency $1/f$ noise as well as high $\sim f^2$ capacitance noise on top of white thermal noise and shot noise. (Inset) The electrical current histogram fit with a Gaussian distribution (mean = 6.57 ± 0.03 nA, width = 0.77 ± 0.07 , $\chi^2 = 2.25$). (b) The optical noise spectra, virtually flat from 5 to 100 kHz. (Inset) The optical current histogram fit with a Poisson distribution (mean = 5.55 ± 0.01 cnts/ $4 \mu\text{s}$, $\chi^2 = 0.96$). (c) SNR for the optical signals as a function of the bandwidth evaluated using: $SNR = I_{avg} / I_{RMS}(BW)$, $I_{RMS}(BW) = \sqrt{\int^{BW} PSD df}$ showing positive function of the total number of counts. Adapted with permission from Anderson et al. [53]. Copyright 2014 American Chemical Society.

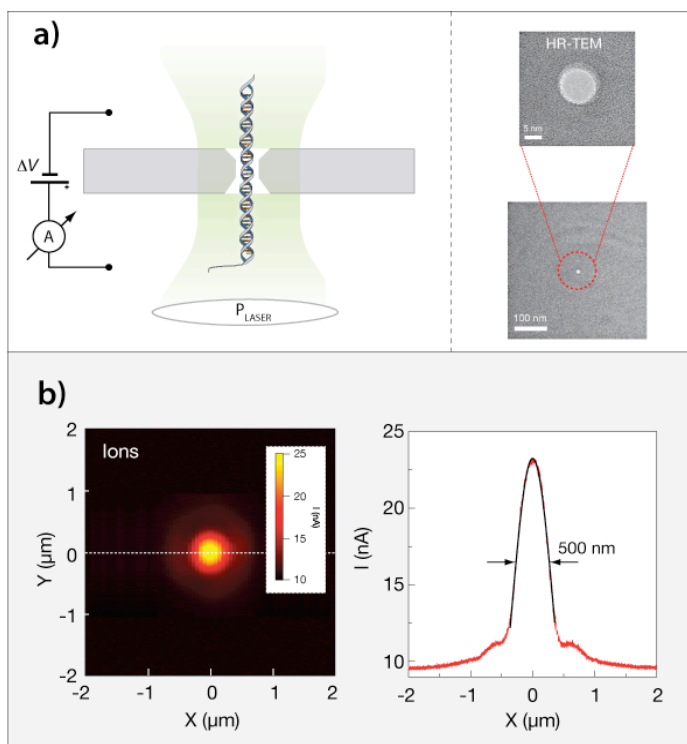


Figure 6 | The optoelectric effect in solid-state nanopores. (a) The green laser is focused on the pore using confocal illumination and the electrical current is measured using a pair of Ag/AgCl electrodes. TEM image on a 10 nm pore on the right. (b) Surface plot of the current measured while a $4 \times 4 \mu\text{m}^2$ region on the membrane is scanned using a focused 10 mW green laser beam at $1 \mu\text{m}/\text{s}$. When the laser beam overlaps the nanopore a significant current enhancement is observed. Reprinted with permission from Macmillan Publishers Ltd: Nature Nanotechnology, Di Fiori et al. [41], copyright 2013.

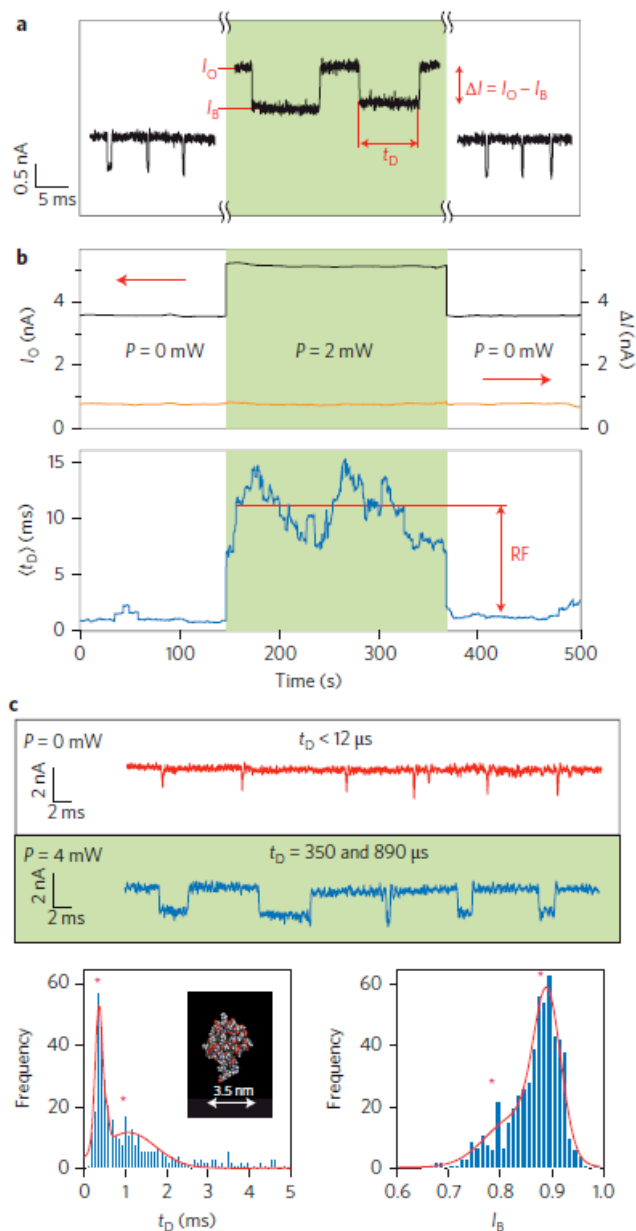
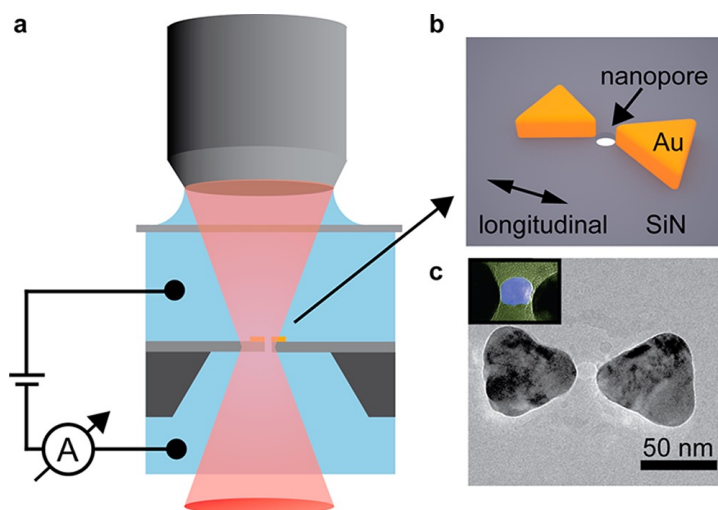


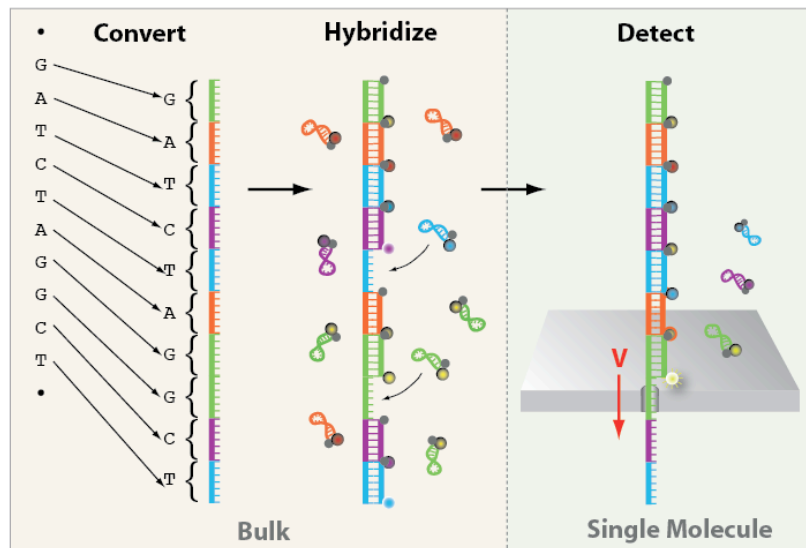
Figure 7 | Slowing down the translocation speed of DNA molecules and proteins using light. (a) Translocation events of 10 kbp DNA molecules in a 5.4 nm nanopore. Once a 2 mW laser beam (pre-aligned with the nanopore) is switched on, the open pore current (I_O), the blockade current (I_B) and translocation time (t_D) increase. The blocked current amplitude (ΔI) remains constant. (b) Traces of the open-pore current (I_O), blocked current amplitude (ΔI) and the mean translocation time ($\langle t_D \rangle$) as a function of time. $\langle t_D \rangle$ represent a running average over 150 translocation events, initialized at the moment the laser is switched on/off. (c) Translocation events of ubiquitin, a small-molecular-weight protein, in its native state in a 5 nm pore. Two orders of magnitude increase in the translocation time is observed under illumination of 4 mW focused laser (blue line) in comparison to the translocations recorded before switching on the laser (red line). Histograms of the translocation time (t_D) and fractional blockade current (I_B) calculated

1
2
3
4 using more than 500 events. The results show two prominent timescales for ubiquitin
5 translocation time (340 ± 5 ms and 890 ± 70 ms), as well as two peaks in the blockade
6 currents (0.88 and 0.78), approximated by a sum of two Gaussians (red lines). Inset:
7 Crystallographic structure of wild-type human ubiquitin (PDB 1d3z). Reprinted with
8 permission from Macmillan Publishers Ltd: Nature Nanotechnology, Di Fiori et al.[41],
9 copyright 2013.
10
11
12
13
14
15
16
17
18
19
20
21
22
23
24
25
26
27
28
29
30
31
32
33



34 Figure 8 | The principle of plasmonic nanopore optical profiling. (a) Schematic illustration
35 of the measurement set up. A 785 nm laser was focused into a flow cell, the position of
36 the flow cell was controlled using a piezo stage to allow three dimensional scanning. The
37 variations in the optical intensity within a focal zone caused temperature changes in the
38 nanoplasmonic structure that were measured electrically through changes in the ionic
39 conductance. (b) Three dimensional schematic illustration of the plasmonic bowtie
40 nanoantenna with a nanopore in the gap. (c) TEM image of the plasmonic nanopore
41 showing the plasmonic antenna consisting of two gold nanotriangles separated by a 10
42 nm gap in which a 10 nm nanopore was drilled. Adapted with permission from Jonsson et
43 al. [60]. Copyright 2013 American Chemical Society.
44
45
46
47
48
49
50
51
52
53
54
55
56
57
58
59
60

a)



b)

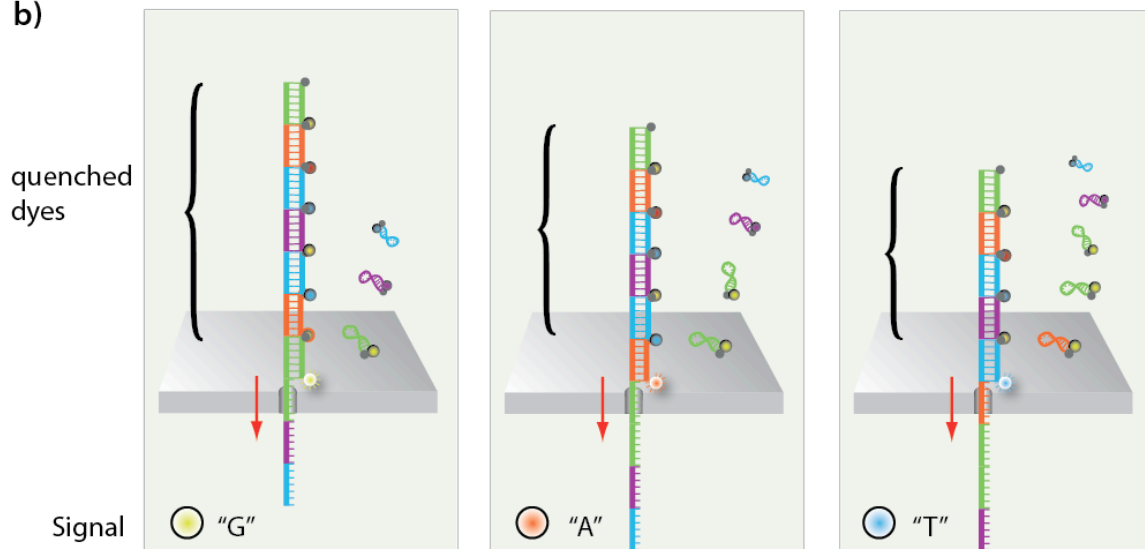


Figure 9 | Schematic Illustration of the optical sequencing method. Each base is converted to an extended sequence that is hybridized to a fluorophore-quencher beacon, where each base is represented by a different fluorophore color. The DNA/beacon complex is then threaded through a nanopore and the color barcode is detected optically. Each released beacon is automatically closed, quenching its own fluorescence while diffusing away from the vicinity of the pore.

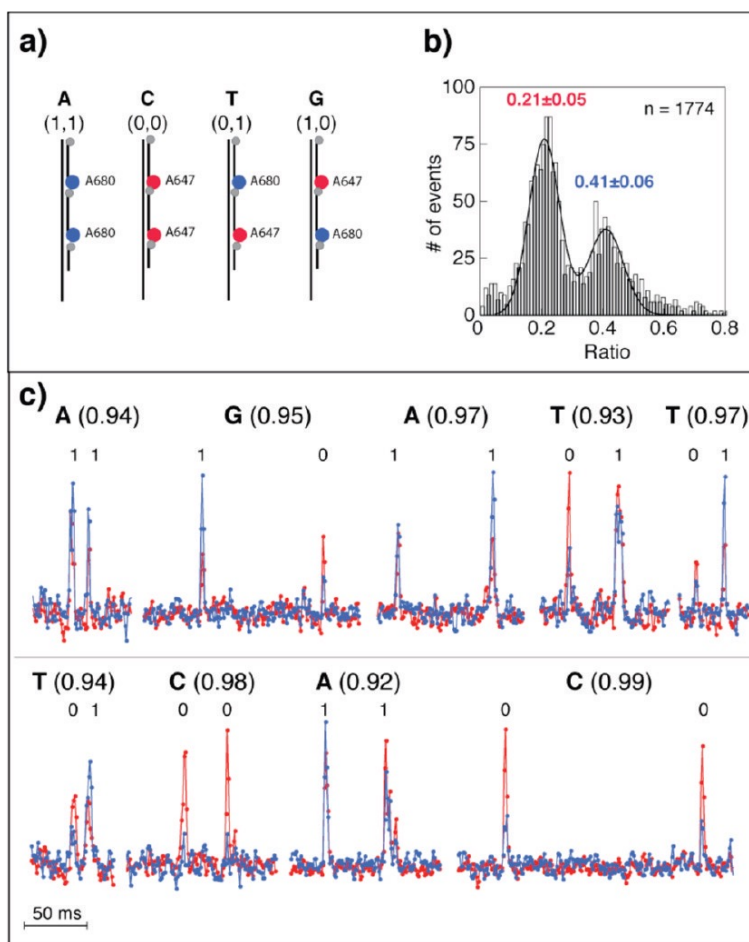


Figure 10 | Optical detection of the four 2-bit combinations representing the four different nucleotides. (a) Illustration of the four samples labeled with two fluorophores correspond to the four bases. (b) The color ratio (R) distribution of 1774 events revealing two peaks corresponding to the two fluorophores. (c) Representative intensity corrected fluorescence traces of unzipping events. Corresponding bit called, base called, and certainty score indicated above the event. The intensities in the two channels were corrected automatically by a computer code after each bit is called using a fixed threshold R value. Adapted with permission from McNally et al. [16]. Copyright 2010 American Chemical Society.

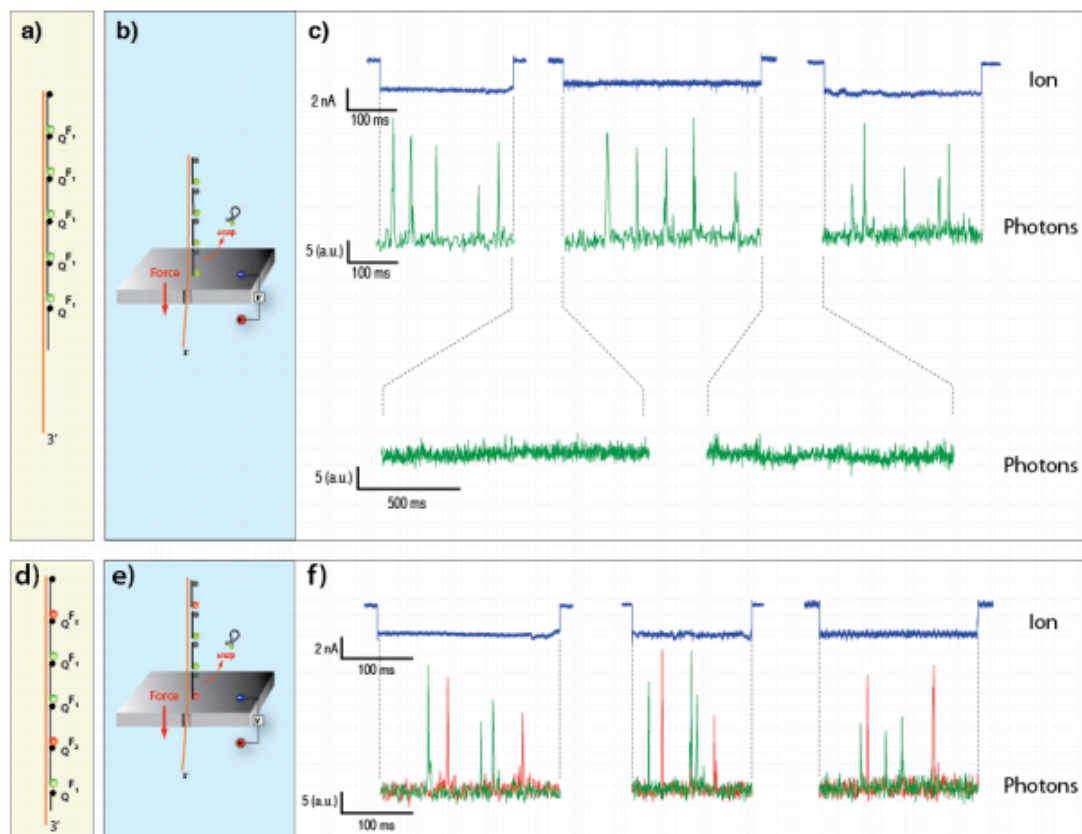


Figure 11 | Single and dual color barcode detection using low PL nanopore. (a,d) Illustration of the ssDNA template consisting of 16-mer binding sequences hybridized to molecular fluorophore-quencher labeled beacons. Each DNA strand is labeled with either five green ("F1") fluorophores (a) or specific sequence of green and red ("F1" and "F2", respectively) fluorophores (d) as well as a quencher oligo. The strands are threaded through a low PL, 3 nm nanopores. The marked beacons are stripped off one at the time creating a distinct fluorescent burst (b,e). The electrical and optical signals are measured simultaneously, showing five clear photon bursts per event in the green channel (c) or green and red channels (f) according to the sample. Adapted with permission from Assad et al.[47]. Copyright 2014 American Chemical Society.